Available online www.jocpr.com

Journal of Chemical and Pharmaceutical Research, 2018, 10(4): 16-23

Research Article

ISSN : 0975-7384
CODEN(USA) : JCPRC5

Synthesis of Plasma-Modified Mo-TiO_2 for Photocatalytic Degradation of Gaseous Toluene

Haosu Cao[1,2], Changjun Zhu[1,2], Kaige Chen[1,2], Fujiao Song[2] and Qi Xu[2*]

[1]*School of Environmental and Safety Engineering, Changzhou University, Changzhou, P R China*
[2]*School of Chemistry and Chemical Engineering, Yancheng Institute of Technology, Yancheng, P R China*

ABSTRACT

Nanostructured TiO_2 and Mo-TiO_2 were prepared by a sol–gel method at ambient temperature, and plasma-modified Mo-TiO_2 and TiO_2 were prepared by modification using non-thermal plasma. The as-prepared catalysts were characterized by XRD, BET, SEM, TEM, XPS and UV-Vis DRS. XRD results indicated that the TiO_2 and Mo-TiO_2 lattice structures had no change except for the crystal size after plasma treatment. SEM images indicated that plasma-treated catalysts exhibit better dispersibility. The BET analysis of the plasma-treated catalysts indicated a larger specific surface area and pore diameter. XPS results confirmed that Mo had been doped into the TiO_2 lattice, and the characteristic peaks shifted to higher energy after plasma treatment. UV-Vis DRS analysis of the doped and plasma-treated TiO_2 photocatalytic materials indicated a red-shift of absorption to the visible region. Toluene, which is a typical volatile organic compound (VOC), was chosen as a model air pollutant. The photocatalytic activities of prepared photocatalysts were investigated in a gas–solid photoreactor for the decomposition of gaseous toluene. Results indicated that materials modified by non-thermal plasma exhibit higher photocatalytic activities.

Keywords: Non-thermal plasma; Photocatalysis; Volatile organic compound; Sol-gel method

---

INTRODUCTION

The modernization of economy and industry has led to a major issue of air pollution in several areas [1]. Volatile organic compounds (VOCs) are regarded as one of the most significant air pollutants caused by human activity [2]. VOCs include hazardous substances, which are predominantly responsible for the formation of smog and ozone precursors. In addition, these compounds are suspected to be pathogenic factors of cancer, which can render temporary or permanent toxic effects on the hematological, respiratory, and liver systems, as well as other organs in the human body, and cause severe threat to the human living environment and even our survival [3]. The main components of VOCs include benzene homologs, where toluene is a typical compound [4]. With increasing concerns on the harm of toluene to human in the air, especially the indoor atmosphere, the treatment of toluene is attracting immense interest. Several studies have been conducted to find an efficient, convenient, and low-cost photocatalyst for the decomposition of gaseous toluene in air at room temperature [5-8]. From an in-depth study using TiO_2 semiconductors reported previously, the absorption wavelength of TiO_2 shifts from the ultraviolet to the visible-light region [9], demonstrating potential in photocatalysis. Studies reported in related fields have explored different methods for decreasing the band gap of TiO_2 so as to observe an optical response in the visible range [10-13]. To extend the absorption of TiO_2 in the visible range so as to completely exploit solar energy, doping using impurities is the typical modification method for sensitizing the property of TiO_2. A number of studies have demonstrated that the doping of TiO_2 improves its absorption property to visible light [14-16]. However, the enhancement of visible-light absorption has been reported to not sufficiently increase the catalytic activity [17,18].

Plasma is gas in the ionized state, which contains a large number of electrons, ions, neutral atoms, excited atoms, photons, and free radicals, and of these components, the electronic charge is numerically equal to the positive charge. During the doping of TiO_2 by the traditional sol–gel method, contaminants can be introduced into the surface or interstitial sites of the TiO_2 lattice, which can act as defects and recombination centers, lead to the rapid recombination of photoinduced electrons and holes, and decrease photon efficiency. To prevent the inactivation of photocatalysts, some new techniques, e.g., plasma treatment as well as ultrasound and microwave irradiation, have been reported, with constructive results [19,20]. Non-thermal plasma treatment is satisfactory because it is a high-energy, low-cost, energy-efficient application [21,22].

In this study, TiO_2 and Mo-TiO_2 photocatalysts were prepared by a conventional sol–gel method, followed by moisture removal and calcination for crystallization. Next, the prepared samples were treated by non-thermal plasma for a specific time. The plasma-treated catalysts exhibited better photocatalytic activity for the decomposition of gaseous toluene.

EXPERIMENTAL SECTION

Preparation of TiO_2

First, 10 mL of butyl titanate and 2 mL of acetylacetonate (ACAC) were added into 50 mL of ethanol to prepare a mixed solution. Second, 2 g of cetyltrimethylammonium bromide (CTAB) and 3 g of glucose ($C_6H_{12}O_6$) were stirred at room temperature for 30 min to obtain solution "A." Third, 2 mL of deionized water was added into 25 mL of ethanol, and the pH was adjusted to 4–6 by nitric acid (65% wt), followed by thorough stirring to obtain solution "B." Next, solution "B" was added dropwise into solution "A" to ensure slow hydrolysis for butyl titanate. The mixture was stirred for another hour, affording a light-yellow uniform transparent TiO_2 sol after drop ended. Next, the sol was aged at room temperature for 24 h, affording a TiO_2 wet gel. Finally, the gel was completely dried in a vacuum oven for 12 h at 80°C, affording a xerogel, followed by the grinding of samples and sieving into powders. These powders were calcined for 5 h at 500°C, affording anatase TiO_2.

Preparation of Mo-TiO_2

Mo-TiO_2 nanoparticles were prepared by the addition of ammonium molybdate ($(NH_4)_6Mo_7O_{24}\cdot 4H_2O$, A.R.) into solution "B" as the Mo precursor. All remaining steps were the same as those utilized for the preparation of pure TiO_2.

Non-Thermal Plasma Treatment

The prepared TiO_2 and Mo-TiO_2 samples were modified using non-thermal plasma for 30 min. Ar was used for the glow discharge, with a treatment pressure of 30–40 Pa and a power of 36 W.

Catalyst Characterization

The crystalline phase of the samples was investigated by X-ray diffraction (XRD) using a DX-2700 diffractometer utilizing Cu Kα radiation (λ = 0.15406 nm). The morphology of the catalysts was observed by transmission electron microscopy (TEM) using a CM120 system (Philips, The Netherlands). Specific surface areas were determined by BET analysis using an ASAP 2020M system (Micromeritics, USA) at 77 K. X-ray photoelectron spectroscopy (XPS) was employed to investigate the chemical composition of the samples. UV–Vis diffuse reflectance spectra (UV–Vis DRS) were recorded on a UV-2600 (Shimadzu, Japan) system. The photoabsorption property of the powders was recorded using $BaSO_4$ tablet as the reference.

Photocatalytic Degradation of Toluene

Toluene was chosen as a typical VOC in air to evaluate the photocatalytic performance of the samples. The photocatalysts were uniformly tiled in a rectangular quartz reactor under light irradiation. Simulated sunlight was generated using a high-pressure xenon lamp (HPXL, 500 W). The light source and reactor were cooled using circulating water (50 ± 5°C). The toluene concentration was analyzed by a GC 6890N system (Agilent, USA) with an HP-5 column using N_2 as the carrier and H_2 for burning.

RESULT AND DISCUSSION

Catalyst Characterization

XRD and BET analysis:

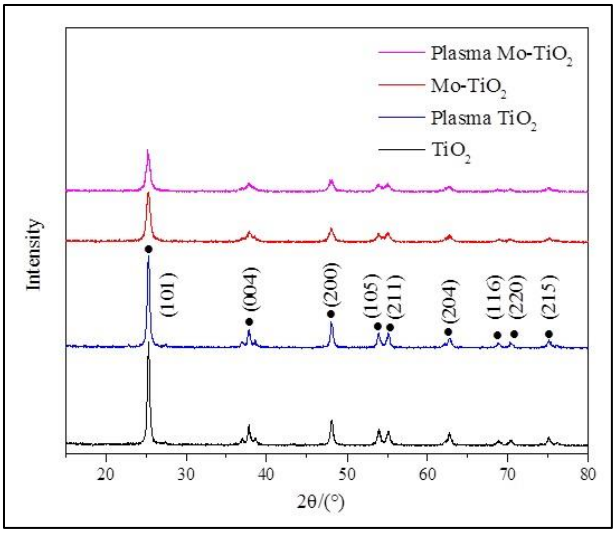

Figure 1: XRD patterns of the catalysts

Figure 1 shows the XRD spectra of the as-prepared photocatalysts. Similar diffraction curves were observed for all samples. Characteristic peaks were observed at 25.3°, 37.8°, 48.2°, 54.2°, 55.2°, 62.7°, 68.6°, 70.5°, and 75.1°, corresponding to the (101), (004), (200), (105), (211), (204), (116), (220), and (215) crystalline planes of the anatase TiO_2 surface, respectively (JCPDS card No. 21-1272) [23]. A diffraction peak corresponding to the Mo phase was not observed, caused by the similar ionic radii of Mo and Ti; hence, Mo can be easily substituted into the TiO_2 lattice without any change in the TiO_2 crystal phase. After doping and plasma treatment, the peaks corresponding to the catalysts were weaker and wider as compared with those corresponding to pure TiO_2. Particularly, after plasma treatment, Mo-TiO_2 exhibited the widest, weakest peaks for anatase, indicating higher lattice disorder and a smaller crystal size. The Scherrer equation and BET analysis were utilized to calculate the physiochemical properties of the samples. Table 1 shows the results. As can be observed from Table 1, the crystal size decreased after plasma treatment. The specific surface area, total pore volume, and average pore diameter of plasma-treated catalysts increased. After plasma treatment, the pollutants attached to the catalyst surface and present in the lattice gap were removed, resulting in better texture.

Table 1: Physiochemical properties of the catalysts

Sample	Crystal size (nm)	Specific surface area (m^2/g)	Total pore volume (cm^3/g)	Average pore diameter (Å)
TiO_2	23	20.1	0.21	106.1
Plasma TiO_2	18.2	30.1	0.25	205.1
Mo-TiO_2	17.5	29.6	0.17	218.1
Plasma Mo-TiO_2	16.8	38.7	0.19	276.3

XPS analysis:

Figure 2 shows the XPS spectra of Survey (a), Ti 2p (b), O 1s (c), and Mo 3d (d) peaks in the prepared catalysts. The electron binding energy was calibrated using C1s (284.6 eV) as the reference. As can be observed from the graph, the characteristic peaks observed at around 459.0 eV and 464.8 eV were typical of Ti $2P_{3/2}$ and Ti $2P_{1/2}$ for the Ti ion, respectively. Binding energy of 530.5eV could be attributed to the O 1s of O-Ti bond from the TiO_2 lattice. Binding energies of 232.5 eV and 235.9 eV corresponded to the Mo $3d_{5/2}$ and Mo $3d_{3/2}$ peaks of the Mo ion, respectively [24]. The binding energy of the peaks shifted to high electric potentials, with the peak intensity increasing with plasma treatment, indicating that the ionic strength is enhanced after plasma treatment, possibly caused by the generation of excited particles in the plasma that remove the contaminating electrons and organics. Hence, the number of active sites increases and catalyst performance is promoted.

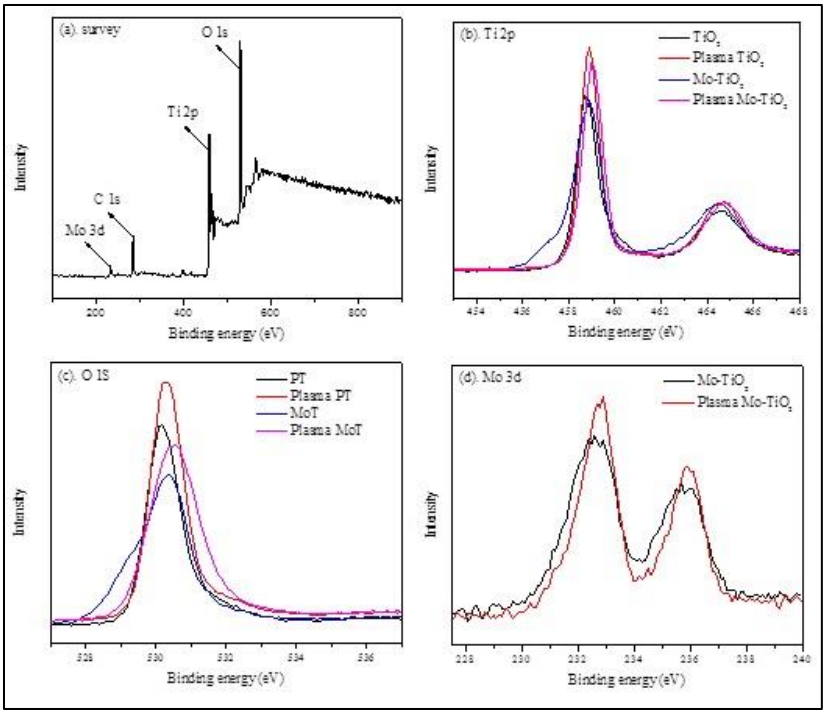

Figure 2: XPS spectra of Survey (a), Ti 2p (b), O 1s (c), and Mo 3d (d) peaks of the catalysts

SEM morphology:

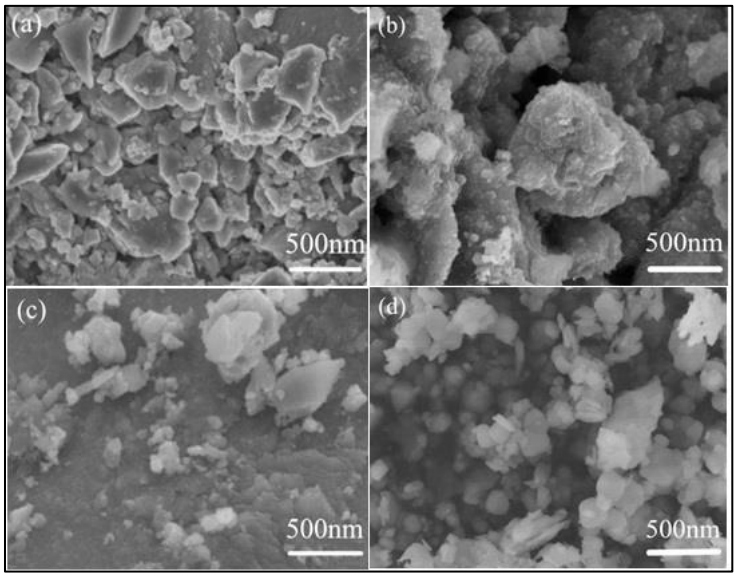

Figure 3: SEM images of the (a) TiO_2, (b) plasma TiO_2, (c) Mo-TiO_2, (d) plasma Mo-TiO_2 catalysts

Figure 3 is the SEM morphology of the prepared catalyst before and after low temperature plasma modification. As from the images, before plasma treatment, the catalysts exhibited aggregated structures with layered and massive blocks, large gaps and spaces were observed between the blocks. However, with plasma treatment, the catalysts exhibited a better dispersed porous structure, and large blocks transformed into small particles. This may be due to the high energy particles in the plasma which could effectively remove pollutants attached to the catalyst surface. Moreover, scatter the particles, change the dispersion of the catalysts and increase the specific surface area.

TEM morphology:

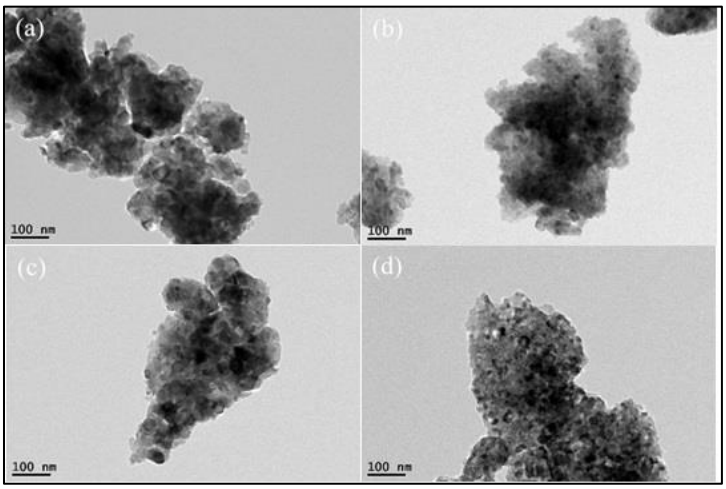

Figure 4: TEM images of the (a) TiO_2, (b) plasma TiO_2, (c) Mo-TiO_2, (d) plasma Mo-TiO_2 catalysts

Figure 4 shows the TEM images of the catalysts. As can be seen from the images, the samples are composed of small particles with average size of 10~30nm. Which was consistent with the results that calculated by the Scherrer equation.

UV-Vis DRS analysis:

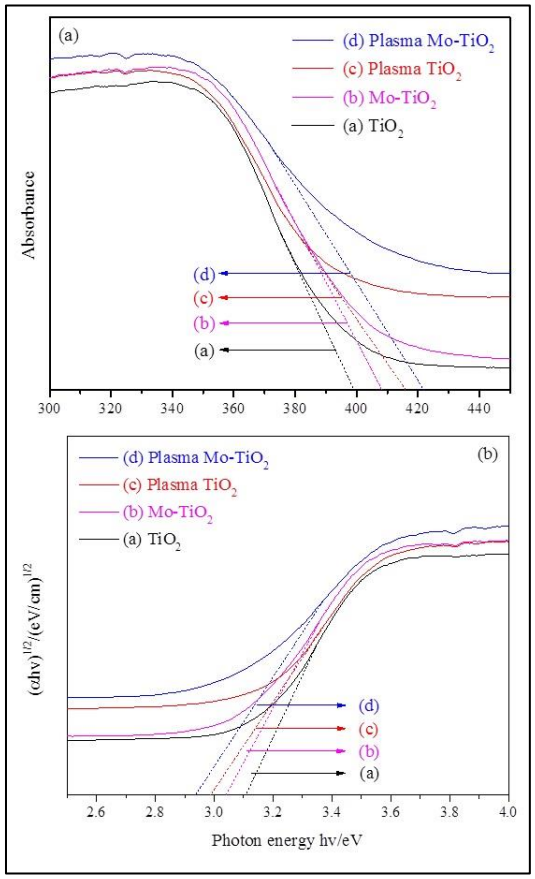

Figure 4: (a) UV-Vis DRS spectra and; (b) Tauc plot of the catalysts

To investigate the optical absorption property of the catalysts, UV–Vis DRS measurements of the samples were conducted. Figure 4 (a) shows the absorption curve spectra of the catalyst samples. The absorption band

corresponding to plasma TiO_2 and Mo-TiO_2 shifted to a higher absorption wavelength of visible light as compared with that of the untreated catalysts. Generally, the band gap of semiconductors is related to the absorption wavelength, and the Tauc plot [25] curve of the $(\alpha hv)^{1/2}$ – hv can be obtained by the calculation of the optical absorption data using the Kubelka–Munk equation [26]. As can be observed from the Tauc plot, the band gap of the catalysts was inversely proportional to the absorption wavelength: catalysts with a narrow band gap were excited by visible light. As a result, the band gap of the catalysts subjected to plasma treatment is less than those of untreated TiO_2 and Mo-TiO_2. Table 2 summarizes the absorption edge and band gap of the catalysts. Particularly, plasma Mo-TiO_2 exhibited a band gap energy of 2.94 eV, which was less than those of other catalysts. Previous studies have confirmed that doping with Mo possibly enhances the visible absorption property of TiO_2 [27]. When the catalysts are exposed to the plasma atmosphere, several excited particles impinge on their surfaces. As mentioned above, these energetic particles are capable of cleaning the catalyst surface or gaps and breaking massive blocks into small particles. Hence, the number of free radicals on the catalyst surface increases, consequently promoting the optical absorption property of visible light. With the enhancement of the visible absorption, the photoelectric quantum efficiency of TiO_2 can be enhanced because of the high generation of photoinduced electrons and holes in the photocatalytic process.

Table 2: Absorption edge and band gap of the catalysts

	TiO_2	Mo-TiO_2	Plasma TiO_2	Plasma Mo-TiO_2
Absorption edge (nm)	398.7	407.9	416.1	421.8
Band gap (eV)	3.11	3.04	2.98	2.94

Comparative Study of Photocatalytic activity of the Catalysts

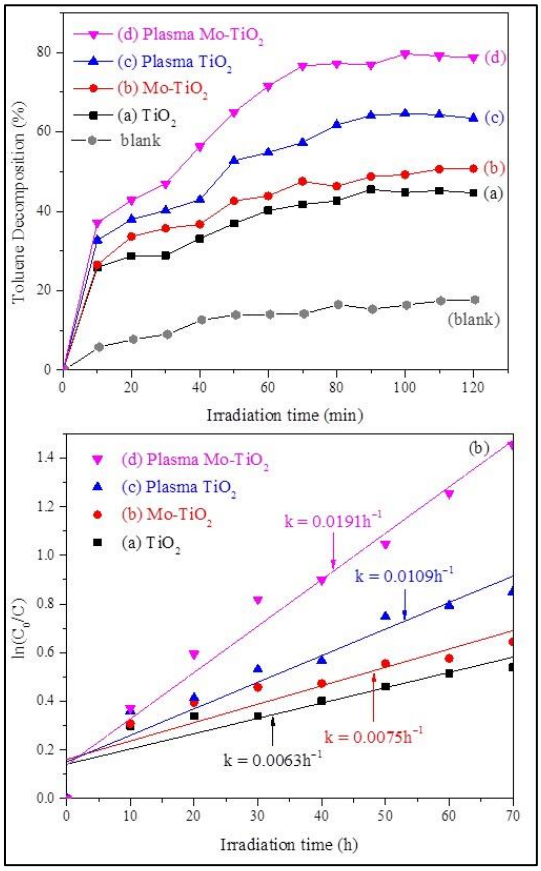

Figure 4: (a) Variation of the decomposition efficiency of toluene over the catalysts under visible-light irradiation (b) Variation of ln(C_0/C) of toluene over the catalysts under visible-light irradiation

Figure 4(a) shows the photocatalytic decomposition efficiency of gaseous toluene over different catalysts (i.e., blank, pure TiO_2, Mo-TiO_2, plasma TiO_2, and plasma Mo-TiO_2) under visible-light irradiation. Simulated toluene gas was generated from a high-pressure cylinder of high-purity air injected with toluene vapor. The flow rate was 100 mL/min, the toluene initial concentration was 100 ppm, and the relative humidity was regulated at 35 ± 5% by water evaporation. As can be observed from the figure, the toluene decomposition efficiency for all samples increased over the irradiation time and was gradually maintained steady after 80 min. A plateau was observed from 20 min to 30 min, possibly associated with the desorption of the toluene adsorbed on the catalysts with increasing temperature under irradiation. Different catalysts exhibited different photocatalytic activities. In particular, the toluene decomposition efficiencies for all catalysts under visible light followed the order of plasma Mo-TiO_2 > plasma TiO_2 > Mo-TiO_2 > TiO_2. For plasma Mo-TiO_2, the toluene decomposition efficiency rapidly increased over the irradiation time and attained the highest stable value at around 80%.

Previous studies have reported that the photocatalytic degradation of VOCs is regarded as the pseudo first-order reaction [28,29]. The kinetic rate of the process can be expressed as the Langmuir–Hinshelwood model:

$$\ln\ (C_0 / C)\ =\ kt\ +\ b$$

Here, C_0 is the initial toluene concentration at t = 0, C is the residual toluene concentration at t, and k is the rate constant of the reaction. Figure 4(b) shows the curve of $\ln(C_0/C)$ versus the irradiation time of toluene over the catalysts with visible-light irradiation. The photocatalytic degradation rate of toluene can be expressed by the slope of the straight line. As can be observed from the figure, the reaction rate constants for TiO_2, Mo-TiO_2, plasma TiO_2, and plasma Mo-TiO_2 were 0.0063, 0.0076, 0.0109, and 0.0190, respectively. The photocatalytic activity of plasma Mo-TiO_2 was clearly greater than those of other samples, which is approximately three times that of TiO_2.

The high photocatalytic activity for plasma Mo-TiO_2 is possibly caused by synergistic effects of Mo doping and non-thermal plasma. On the one hand, with the doping of Mo into the TiO_2 lattice, mid band gaps between the valence and conduction bands are possibly generated, the band gap width of samples shifted to the visible region; hence, the light-absorption range by samples is effectively enhanced, which promotes the photoinduced quantum efficiency of solar light illumination. On the other hand, the special interface in the catalyst prepared by plasma not only can improve the physiochemical property of Mo ions and the TiO_2 semiconductor but also increase the transfer and resolution efficiencies of the photoinduced electrons and holes. In addition, plasma-treated catalysts exhibited better dispersibility, stability, and optical absorption property; thus, photocatalytic efficiency is significantly promoted.

Because of the complexity of plasma, the reaction mechanism for the plasma treatment of catalysts is still not clear. From characterization data, plasma catalysts exhibit a small crystal size, large specific surface area, and agglomeration after calcination. Hence, when the plasma is in complete contact with the catalysts, the excited particles in plasma can be attached on the catalyst surface and form a plasma layer. The internal electric field will positively affect the catalysts and promote the efficiency of photon collection. In addition, the plasma layer on the nanoparticles can repel each other and improve the dispersion of catalysts, thereby promoting the photocatalytic efficiency.

CONCLUSION

Nanostructured-plasma Mo-doped TiO_2 photocatalysts were synthesized by the sol–gel method and non-thermal plasma treatment. Furthermore, the prepared catalysts were applied to the decomposition of toluene under visible light. The photocatalytic activity of plasma Mo-TiO_2 was greater than those of TiO_2, Mo-TiO_2, and plasma TiO_2. Characterization results indicated that the properties (crystal size, specific surface area, dispersibility, and optical absorption) of plasma Mo-TiO_2 are superior than those of other catalysts, which are beneficial for visible-light photocatalysis. The high photocatalytic efficiency of plasma Mo-TiO_2 was related to the synergism of Mo doping and plasma treatment. Plasma technology can obviously improve the physiochemical properties of the catalysts, as well as demonstrates promise for applications in solving environmental problems.

ACKNOWLEDGEMENTS

This work was supported by the National Key Research and Development Program of China [Grant No. 2016YFC0209203]; the Jiangsu Provincial Environme05ntal Science Research Project of China [Grant No. 2015007]; the Jiangsu Collaborative Innovation Center for Ecological Building Materials and Environmental Protection Equipment Research Project of China [Grant No. CP201504].

REFERENCES

[1] Y Wang; X Ren; D Ji; J Zhang; J Sun; F Wu. *J Environ Sci-China*. **2012**, 24, 95-101.
[2] RR Bansode; JN Losso; WE Marshall; RM Rao; RJ Portier. *Bioresource Technol*. **2003**, 90, 175-184.
[3] HL Chiang; WH Lin; JS Lai; WC Wang. *J Environ Sci Heal A*. **2010**, 45, 1397-1405.
[4] JEC Lerner; EY Sanchez; JE Sambeth; A Porta. *Argentina Atmos Environ*. **2012**, 55, 440-447.
[5] IS Moon; HS Seo; KJ Kim; SH Jang; WJ Jeong; SL Moon; HR Lee; MC Chung; SK Cho; SC Jung; HG Ahn. *J Nanosci Nanotechnol*. **2011**, 11, 7382-7385.
[6] H Huang; W Li. *Appl Catal B-Environ*. **2011**, 102, 449-453.
[7] Z Wei; J Sun; Z Xie; M Liang; S Chen. *J Hazard Mater*. **2010**, 177, 814-821.
[8] H Huang; DYC Leung; G Li; MKH Leung; X Fu. *Catal Today*. **2011**, 175, 310-315.
[9] J Ouyang; M Chang; X Li. *J Mater Sci*. **2012**, 47, 4187-4193.
[10] H Wang; JP Lewis. *J Phys Condens Matter*. **2006**, 18, 421-434.
[11] D Robert. *Catal Today*. **2007**, 122, 20-26.
[12] X Yuan, K Qiu, W Tang, Q Liub. Preparation and Photocatalytic Properties of Cu-doped Nano-TiO2/Microcrystal Muscovite Composites[C], International Conference on Machinery, Materials Engineering, Chemical Engineering and Biotechnology. **2016**, 106-111.
[13] Y Wang; J Zhang; L Liu; C Zhu; X Liu; Q Su. *Mater Lett*. **2012**, 75, 95-98.
[14] Y Zhang; X Xiong; Y Han; X Zhang; F Shen; S Deng; H Xiao; X Yang; G Yang; H Peng. *Chemosphere*. **2012**, 88, 145-154.
[15] CD Valentin; E Finazzi; G Pacchioni; A Selloni; S Livraghi; MC Paganini; E Giamello. *Chem Phys*. **2007**, 339, 44-56.
[16] D Chen; Z Jiang; J Geng; Q Wang; D Yang. *Ind Eng Chem Res*. **2007**, 46, 2741-2746.
[17] H Zhang; G Chen; DW Behnemann. *J Mater Chem*. **2009**, 19, 5089-5121.
[18] A Ghicov; B Schmidt; J Kunze; P Schmuki. *Chem Phys Lett*. **2007**, 433, 323-326.
[19] MB Kizling; SG Jaras. *Chem Inform*. **1997**, 28, 1-21.
[20] UR Pillai; E Sahle-Demessie; RS Varma. *Appl Catal A-Gen*. **2003**, 252, 1-8.
[21] CJ Liu; GP Vissokov; WL Jang. *Catal Today*. **2002**, 72, 173-184.
[22] CJ Liu; DG Cheng; YP Zhang; KL Yu; Q Xia; JG Wang; XL Zhu. *Catal Surv Asia*. **2004**, 8, 111-118.
[23] X Wang; RG Li; Q Xu; HX Han; C Li. *Acta Phys-Chim Sin*. **2013**, 29, 1566-1571.
[24] H Al-Kandari; F Al-Kharafi; A Katrib. *Catal Commun*. **2008**, 9, 847-852.
[25] R Rusdi; AA Rahman; NS Mohamed; N Kamarudin; N Kamarulzaman. *Powder Technol*. **2011**, 210, 18-22.
[26] MP Fuller; PR Griffiths. *Anal Chem*. **1978**, 50, 1906-1910.
[27] LG Devi; BN Murthy. *Catalysis Lett.* **2008**, 125, 320-330.
[28] X Li; X Zou; Z Qu; Q Zhao; L Wang. *Chemosphere*. **2011**, 83, 674-679.
[29] BK Sang; SC Hong. *Appl Catal B-Environ*. **2002**, 35, 305-315.